SCIENCE CHINA
Life Sciences

•RESEARCH PAPER•

May 2020 Vol.63 No.5: 712–723
https://doi.org/10.1007/s11427-018-9543-1

# Identification and characterization of two morphologically distinct stem cell subpopulations from human urine samples

An-Jing Chen[1†], Jin-Kui Pi[1†], Jun-Gen Hu[1†], Yi-Zhou Huang[1], Hong-Wei Gao[1], Sheng-Fu Li[2], Jesse Li-Ling[1] & Hui-Qi Xie[1*]

[1]*Laboratory of Stem Cell and Tissue Engineering, State Key Laboratory of Biotherapy and Cancer Center, West China Hospital, Sichuan University and Collaborative Innovation Center of Biotherapy, Chengdu 610041, China;*
[2]*Key Laboratory of Transplant Engineering and Immunology of Ministry of Health, West China Hospital, Sichuan University, Chengdu 610041, China*

Received April 5, 2019; accepted May 6, 2019; published online September 10, 2019

Urine-derived stem cells (USCs) have shown potentials for the treatment of skeletal and urological disorders. Based on published literature and our own data, USCs consist of heterogeneous populations of cells. In this paper, we identify and characterize two morphologically distinct subpopulations of USCs from human urine samples, named as spindle-shaped USCs (SS-USCs) and rice-shaped USCs (RS-USCs) respectively. The two subpopulations showed similar clone-forming efficiency, while SS-USCs featured faster proliferation, higher motility, and greater potential for osteogenic and adipogenic differentiation, RS-USCs showed greater potential for chondrogenic differentiation. POU5F1 was strongly expressed in both subpopulations, but MYC was weakly expressed. Both subpopulations showed similar patterns of CD24, CD29, CD34, CD44, CD73, CD90 and CD105 expression, while a higher percentage of RS-USCs were positive for CD133. SS-USCs were positive for VIM, weakly positive for SLC12A1 and UMOD, and negative for KRT18, NPHS1, AQP1 and AQP2, indicating a renal mesenchyme origin; while RS-USCs are positive for VIM, partially positive for KRT18, NPHS1, AQP1, SLC12A1 and UMOD, and negative for AQP2, indicating a nephron tubule origin. The above results can facilitate understanding of the biological characteristics of subpopulations of USCs, and provide a basis for further research and applications of such cells.

**characterization, cell subpopulation, identification, tissue origin, urine-derived stem cells**

**Citation:** Chen, A.J., Pi, J.K., Hu, J.G., Huang, Y.Z., Gao, H.W., Li, S.F., Li-Ling, J., and Xie, H.Q. (2020). Identification and characterization of two morphologically distinct stem cell subpopulations from human urine samples. Sci China Life Sci 63, 712–723. https://doi.org/10.1007/s11427-018-9543-1

## INTRODUCTION

Stem cell-based therapy and tissue engineering have shown potentials for the repair of various tissues. Many types of stem cells have been used for the repair or regeneration of tissues in animal models employing either trans-differentiation or paracrine effects to stimulate endogenous cells to participate in tissue regeneration. These included embryonic stem cells (ESCs) (Puri and Nagy, 2012), induced pluripotent stem cells (iPSCs) (Puri and Nagy, 2012), multipotent mesenchymal stromal cells (MSCs) (Phinney and Prockop, 2007) including bone marrow-derived mesenchymal stromal cell (BMSCs) (Kuroda, et al., 2011; Huang et al., 2013), adipose-derived stem cells (ADSCs) (Schäffler and Büchler, 2007), and amniotic fluid stem cells (De Coppi et al., 2007). Despite ethical issues and availability, such cells have shown to be effective for repairing and regeneration of tissues.

In addition to aforementioned cell types, urine derived stem cells (USCs) have drawn much attention recently. Many published studies have focused on the biological characteristics and applications of such cells for the treatment of

†Contributed equally to this work
*Corresponding author (email: xiehuiqi@scu.edu.cn)

skeletal and urological disorders (Zhang et al., 2008; Bharadwaj et al., 2011; Bharadwaj et al., 2013; Guan et al., 2014; Pei et al., 2014; Zhang et al., 2014; Guan et al., 2015; Schosserer et al., 2015; Gao et al., 2016; Chen et al., 2017). Due to their minimal ethical issues and easy availability, USCs have shown great advantages for tissue repair.

However, the therapeutic effects largely depend on the intrinsic biological characteristics of stem cells. Adult stem cells usually comprise subpopulations with various characteristics and application potentials. MSCs also have different cell subpopulations with various morphologies and biological characteristics (Han et al., 2017; Huang et al., 2017). Examples include bone marrow mesenchymal stromal cells (BMSCs) (Li et al., 2016; Pérez-Silos et al., 2016), umbilical cord blood stem cells (UCBSCs) (Alvarez-Gonzalez et al., 2013; Ju et al., 2013), and amniotic fluid stem cells (AFSCs) (Bossolasco et al., 2006). Their biological characteristics often result in different tissue repair potentials. For example, subpopulations of stem cells have shown different potentials for osteogenic and chondrogenic differentiation (Pérez-Silos et al., 2016), and effectiveness for the treatment of retinal degeneration (Li et al., 2016).

Based on published literature and our own experience, USCs also have heterogeneous morphologies, which suggests the existence of subpopulations of cells. Zhang et al. firstly reported USCs with progenitor cell characteristics (Zhang et al., 2008). Bharadwaj et al. studied the biological characteristics of stem cells from the upper urethra which have a rice grain-like morphology (Bharadwaj et al., 2011). Guan et al. compared the characteristics of USCs with those of adipose-derived stem cells, and described the USCs as fibroblast-like (Guan et al., 2014). Schosserer et al. described the morphologies of USCs to range from epithelium-like to elongated-fibroblastoid, and observed that after passaging the cells became uniformly elongated-fibroblastoid (Schosserer et al., 2015). In our experience, morphologically distinct urine derived cell types can also be obtained through cell culture.

As USCs may have different characteristics and application potentials, it is necessary to characterize the subpopulations of the urine derived cells in order to provide a basis for further research. In this study, we collected urine derived cell clones by individual digestion (Figure S1 in Supporting Information), and characterized two morphologically distinct subpopulations of USCs.

## RESULTS

### Identification of two morphologically distinct USCs subpopulations

In total 110 urine samples were collected from 15 healthy individuals (1 female and 14 males, ages 3–36 years). Primary cultures of USCs were feasible from urine samples as little as 3 mL. From these samples, epithelial cells (Figure S2 in Supporting Information) and two morphologically distinct USCs subpopulations (as demonstrated by the capabilities of multi-differentiation and expression of stemness-related genes described below) were obtained. One subpopulation had a spindle shape (SS-USCs) with lower refractivity, while the other had a rice-like shape (RS-USCs) with higher refractivity (Figure 1A). The major axis and minor axis were quantitatively measured. As shown in Figure 1B, the major axis of SS-USCs was longer than that of RS-USCs (85.1±20.7 μm and 42.4±9.7 μm, respectively, $P<0.05$), while the minor axes were similar (13.9±4.6 μm and 15.1±2.1 μm, respectively, $P>0.05$). These morphological features were maintained after a series of subcultures (Figure 1C).

### Stemness-related gene expression profiles of SS-USCs and RS-USCs

The expression levels of stemness-related genes, POU5F1 (also known as OCT4) and MYC (also known as c-MYC), were evaluated by RT-qPCR. Urine derived epithelial cells were used as the control. As shown in Figure 2A, both SS-USCs and RS-USCs had higher POU5F1 and MYC expression levels than epithelial cells ($P<0.05$). These results indicated that both SS-USCs and RS-USCs had high expression levels of stemness-related genes in the experimental conditions.

### SS-USCs show greater osteogenic and adipogenic differentiation potentials but less chondrogenic differentiation potential *in vitro*

Both SS-USCs and RS-USCs could differentiate into osteocytes (Figure 2B), adipocytes (Figure 2C), and chondrocytes (Figure 2D), as demonstrated respectively by positive Alizarin red S staining, Oil-red O staining, and Alcian blue staining. Quantitatively (Figure 2E), SS-USCs had a larger staining area of Alizarin red S than RS-USCs (0.042±0.008 $mm^2$ and 0.018±0.002 $mm^2$, respectively, $P<0.05$), a larger staining area of Oil-red O than RS-USCs (0.142±0.020 $mm^2$ and 0.009±0.002 $mm^2$, respectively, $P<0.05$), and a smaller staining area of Alcian blue than RS-USCs (0.262±0.039 $mm^2$ and 0.379±0.037 $mm^2$, respectively, $P<0.05$). These results indicated that osteogenic-induced SS-USCs had more mineralization nodules than osteogenic-induced RS-USCs, and adipogenic-induced SS-USCs had more lipid droplets than adipogenic-induced RS-USCs, while chondrogenic-induced RS-USCs had more glycosaminoglycan sulfate than chondrogenic-induced SS-USCs. The results also demonstrated that both SS-USCs and RS-USCs had stem cell characteristics, but that SS-USCs had stronger osteogenic and adipogenic differentiation po-

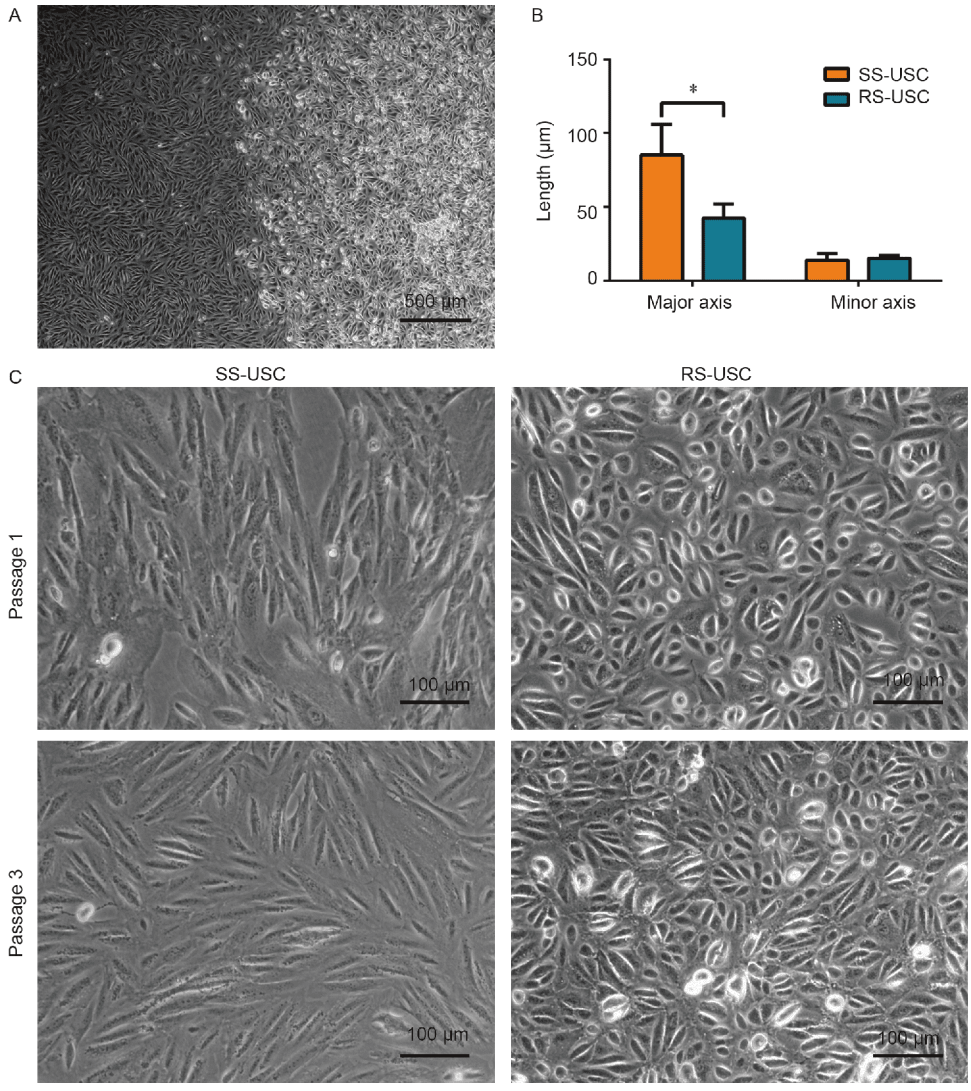


**Figure 1** SS-USCs and RS-USCs had distinct morphologies. A, Morphologically distinct cell clones were observed in primary culture of urine-derived cells. Cells on the left side have a spindle shape, and cells on the right side have a rice-like shape. Scale bar, 500 μm. B, The lengths of the major axis and minor axis of SS-USCs and RS-USCs. SS-USCs had a longer major axis than RS-USCs (*, $P<0.05$). C, SS-USCs have a spindle shape with lower refractivity, and RS-USCs have a rice-like shape with higher refractivity. These morphological features were maintained after subcultures. Scale bar, 100 μm.

tentials, and RS-USCs had a stronger chondrogenic differentiation potential under these experimental conditions.

### SS-USCs display a faster proliferation rate *in vitro*

SS-USCs and RS-USCs were respectively seeded into 96-well plate at 3,000 cells/well. The CCK-8 assay was performed for 6 days, and each day had 6 replicates. The proliferation curve was performed by connecting the $A_{450}$ dots. The SS-USCs had a faster proliferation rate when compared with RS-USCs (Figure 3A).

### SS-USCs and RS-USCs show similar CFE *in vitro*

SS-USCs and RS-USCs were seeded into 25 $cm^2$ culture flasks as 800 cells $cm^{-2}$, respectively. Each type had 4 replicates. After 15 days of culture, the cell clones were fixed with formalin and stained with crystal violet. Cell clones were counted, and CFEs were calculated. Both the SS-USCs and RS-USCs had similar CFEs (2.9%±0.6% and 3.4%±0.4%, respectively, $P>0.05$) (Figure 3B).

### SS-USCs display stronger motility *in vitro*

Motility of the cells was measured with a wound healing assay. SS-USCs and RS-USCs were respectively seeded into 6-well plates at $2\times10^5$ cells/well. When their confluency reached 90%, they were scratched with a 1,000 μL pipette tip. After washing away cell debris, the residual cells were cultured in complete medium containing only 1% FBS for 40 h. The healing rates were calculated. SS-USCs showed a greater healing rate compared with RS-USCs (93.3%±0.4%

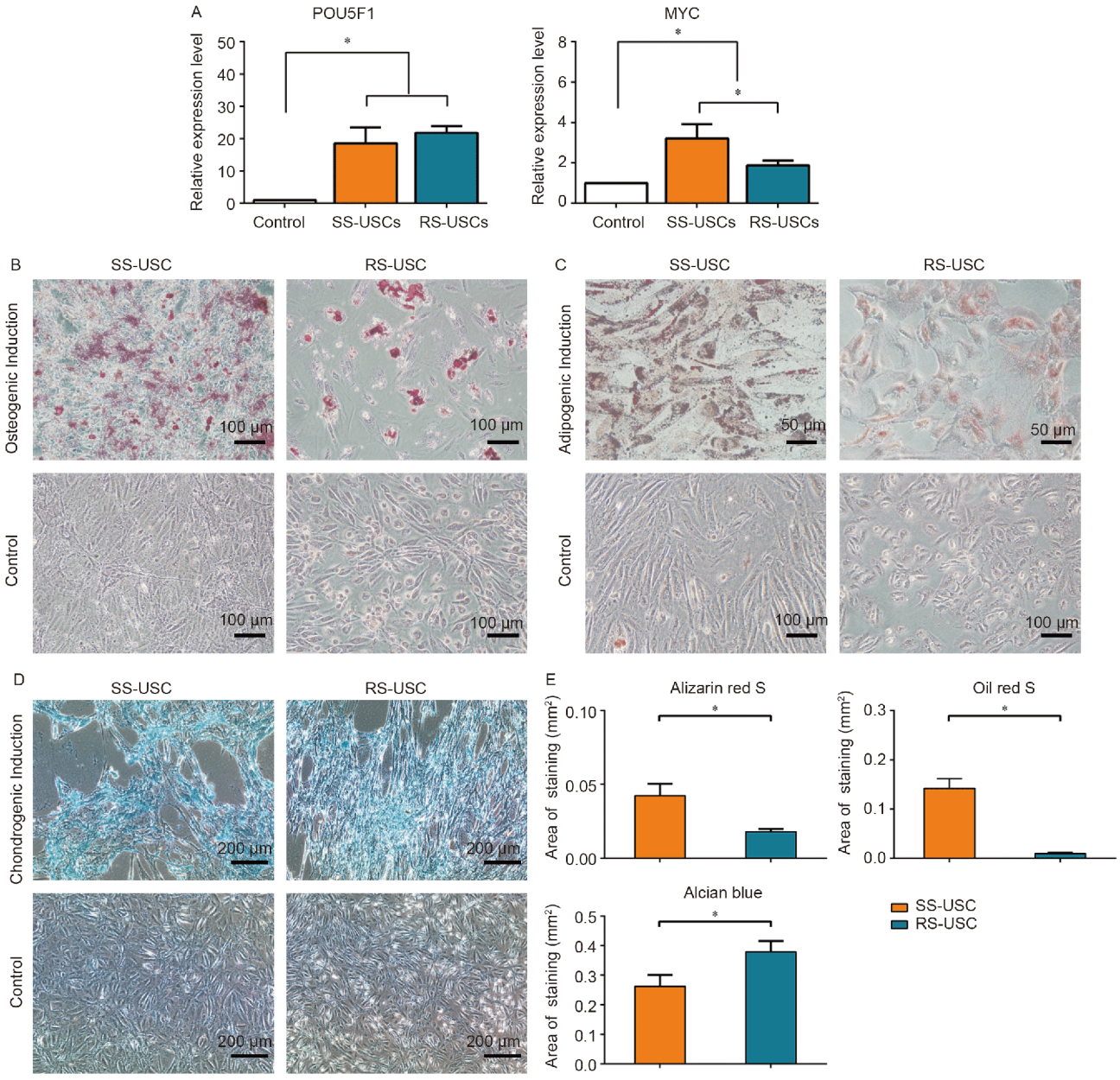


**Figure 2** Multiple differentiation of SS-USCs and RS-USCs. A, Both SS-USCs and RS-USCs had higher expression levels of POU5F1 and MYC than urine derived epithelial cells. *, $P<0.05$. B, Representative images of osteo-differentiation of SS-USCs and RS-USCs by Alizarin red S staining. Scale bar, 100 μm. C, Representative images of adipo-differentiation of SS-USCs and RS-USCs by Oil red-O staining. Scale bar, 100 μm. D, Representative images of chondro-differentiation of SS-USCs and RS-USCs by Alcian blue staining. Scale bar, 100 μm. E, Quantitative analysis of the staining areas of Alizarin red S, Oil red-O, and Alcian blue. Five random microscopic view fields were chosen for statistical analysis. *, $P<0.05$.

and 42.3%±3.0%, respectively, $P<0.05$) (Figure 3C). These results indicated that SS-USCs had stronger motility *in vitro*.

### Cell surface marker profiles of SS-USCs and RS-USCs

The two subpopulations of USCs were subjected to flow cytometric analysis for cell surface markers. As shown in Figure 4A and B, similar proportions of SS-USCs and RS-USCs were positive for CD24 (94.24%±7.73% and 99.55% ±0.21%, respectively, $P>0.05$), CD29 (99.51%±0.79% and 99.91%±0.09%, respectively, $P>0.05$), CD34 (0.43% ±0.15% and 0.51%±0.38%, respectively, $P>0.05$), CD44 (99.82%±0.27% and 99.83%±0.20%, respectively, $P>0.05$), CD73 (99.67%±0.50% and 99.98%±0.01%, respectively, $P>0.05$), CD90 (73.66%±33.48% and 84.00%±18.96%, respectively, $P>0.05$), and CD105 (63.91%±37.55% and 53.59%±26.43%, respectively, $P>0.05$). However, RS-USCs had a higher percentage of cells positive for CD133 than SS-USCs (23.74%±11.03% and 6.13%±5.29%, respectively, $P<0.05$).

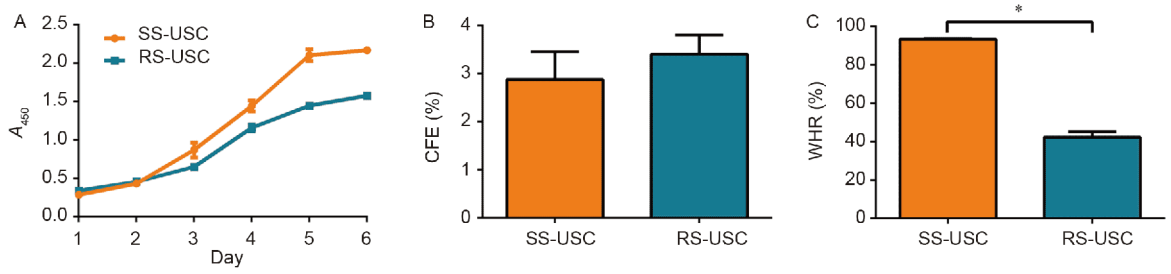


**Figure 3** The proliferation characteristics, clone forming efficiency, wound healing rate and stemness-related genes expression of SS-USCs and RS-USCs. A, The proliferation curves of SS-USCs and RS-USCs. SS-USCs proliferated faster than RS-USCs in the experimental conditions ($P$<0.05). B, SS-USCs and RS-USCs had similar clone forming efficiencies ($P$>0.05). C, SS-USCs had a higher wound healing rate than RS-USCs in the experimental conditions (*, $P$<0.05).

### SS-USCs and RS-USCs may derive from renal mesenchyme and renal tubules, respectively

Delineation of the origin of USCs can enhance the understanding of their biological characteristics. USCs have been reported to be derived from nephron parietal stem cells (Wu et al., 2013). However, morphologically distinct USCs may have different origins, therefore multiple biomarkers for various parts of the nephron were analyzed by immunofluorescence, which included VIM (mesenchyme), KRT18 (urogenital epithelium), NPHS1 (podocyte), AQP1 (proximal cell), SLC12A1 (also known as NKCC2, a marker for the loop of Henle cell), UMOD (also known as THP, a marker for distal convoluted tubule cell), and AQP2 (collecting duct cells) (Lee et al., 2006; Kitamura et al., 2015; Lu et al., 2018).

As shown in Figure 5A, both SS-USCs and RS-USCs had positive stain for VIM. SS-USCs showed negative stain for KRT18, NPHS1, AQP1, and AQP2, and weakly positive stain for SLC12A1 and UMOD. In contrast, a proportion of RS-USCs showed positive stain for KRT18, NPHS1, AQP1, SLC12A1, and UMOD, but few showed positive stain for AQP2. Considering the distribution of such markers in nephrons, SS-USCs may originate from renal mesenchyme near the loop of Henle and the distal convoluted tubule, whereas RS-USCs may originate from the nephron tubules including the Bowman's capsule to the distal convoluted tubule, but not from the collecting duct (Figure 5B).

## DISCUSSION

Stem cells have been widely used in tissue engineering and regenerative medicine. In addition to factors such as scaffolds affecting the tissue engineered transplants (Li et al., 2009; Li et al., 2011; Li et al., 2012; Li et al., 2014; Cao et al., 2018; Han et al., 2018), the intrinsic biological characteristics of stem cells play a critical role. Such cells can exert biological functions in direct and/or indirect ways. They could participate in tissue repair directly and may also secrete various cytokines and extracellular vesicles to motivate other cells (Kuroda et al., 2011). In these cases, the biological characteristics of stem cells become key issues, because different characteristics apply to different situations. USCs are a recently discovered stem cell type (Zhang et al., 2008), which has been studied for potential therapies for urology (Bharadwaj et al., 2011; Bharadwaj et al., 2013), neurology (Guan et al., 2014), bone (Guan et al., 2015), and skeletal muscle (Chen et al., 2017). Morphologically different USCs were reported in these studies, indicating that USCs are not a single cell population. In this study, we identified the subpopulations of USCs and explored their biological characteristics preliminarily.

According to published studies, urine-derived cells have variable types and morphology. Indeed, in our practice of culturing urine-derived cells, three morphologically different cell populations were identified. The first type had a typical epithelial-like morphology but had no potency (Supporting Information), therefore it was regarded as an epithelial cell. The other two populations showed multi-potency and high expression levels of stemness-related genes, indicating that they are stem cells (Figure 2). One has a spindle shaped morphology, which we named SS-USCs. The other has a rice-like shaped morphology, which we named RS-USCs (Figure 1). It was easier to acquire RS-USCs than SS-USCs during the culture process (approximately 70% versus 30%). We evaluated the expression levels of stemness-related genes, POU5F1 and MYC (Figure 2A), which played roles in pluripotency and the fate of stem cells (Klimanskaya et al., 2006). The results showed that SS-USCs and RS-USCs expressed POU5F1 strongly (~20 fold compared to the control) but MYC weakly (~2 fold compared to the control), indicating that the two subpopulations are adult stem cells (Tai et al., 2005), though it is still controversial (Zangrossi et al., 2007). It was also possible that the two subpopulations expressed stemness-related genes due to the presence of growth factors in the culturing environment (Gao et al., 2014). Therefore, their multi-potencies were evaluated. The results show that both types have multi-potencies, but their differentiation abilities vary. SS-USCs has better osteogenic and

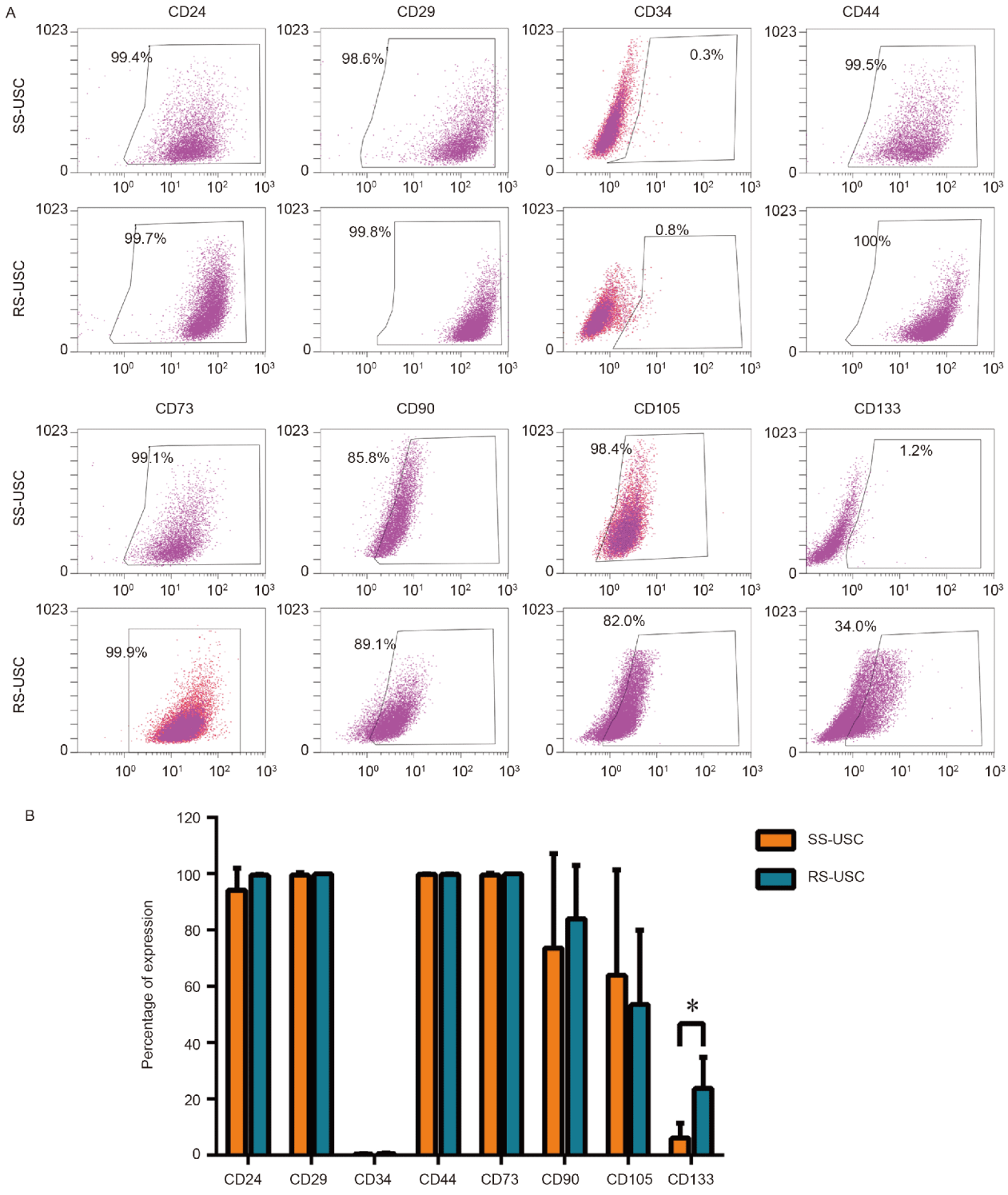


**Figure 4** Flow cytometric analysis for cell surface markers. A, Representative cell surface marker expression profiles of SS-USCs and RS-USCs by FCM analysis. B, Quantitative analysis of cell surface marker expressions of SS-USCs and RS-USCs. Five independent FCM analyses were performed for statistical analysis. *, $P<0.05$.

adipogenic differentiation ability (Figure 2B, C and E), while RS-USCs has better chondrogenic differentiation ability (Figure 2D and E). Besides, the two stem cell subpopulations have comparable clone forming efficiency (Figure 3B), but SS-USCs show a better proliferation rate (Figure 3A) and motility (Figure 3C).

Cell surface markers of SS-USCs and RS-USCs including CD24, CD29, CD34, CD44, CD73, CD90 and CD105 were

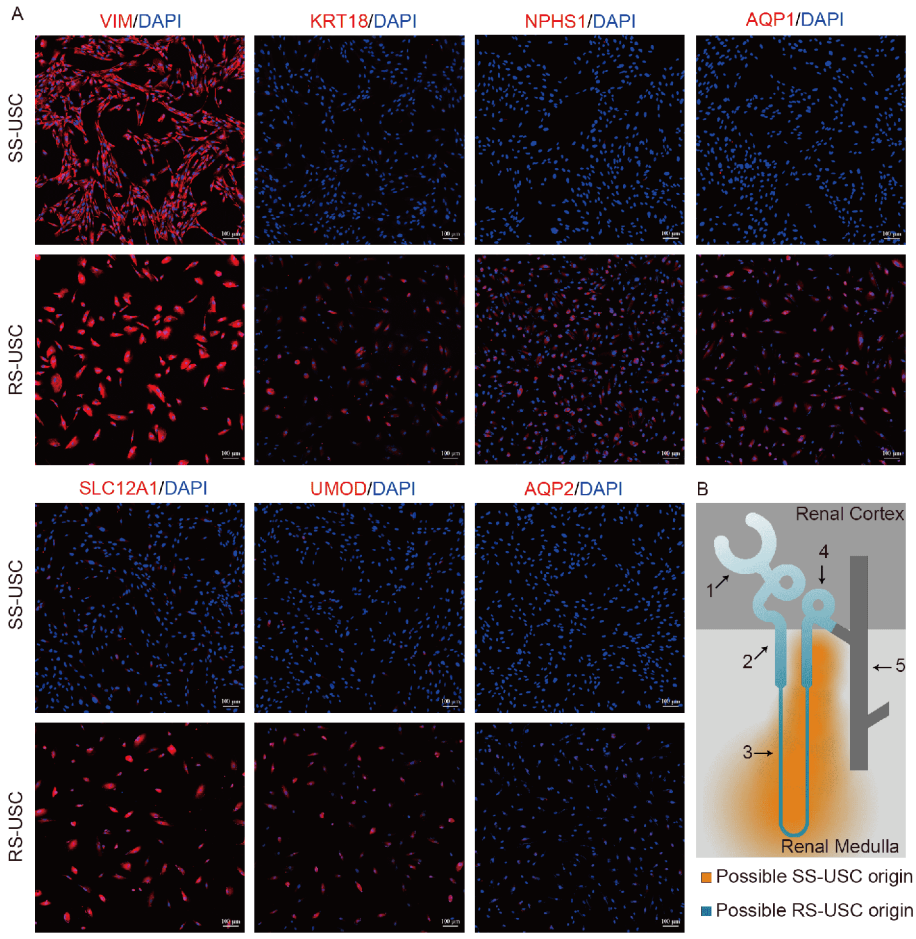


**Figure 5** Possible origins of SS-USCs and RS-USCs as indicated by immunofluorescence. A, Representative immunofluorescence staining for multiple markers of SS-USCs and RS-USCs. Both SS-USCs and RS-USCs were positive for VIM. SS-USCs were negative for KRT18, NPHS1, AQP1, and AQP2, but weakly positive for SLC12A1 and UMOD. Partial RS-USCs cells were positive for KRT18, NPHS1, AQP1, SLC12A1, and UMOD, but few were positive for AQP2. Scale bar, 100 μm. B, Schematic graph of possible origins of SS-USCs and RS-USCs. '1', Bowman's capsule; '2', proximal convoluted tubule; '3', loop of Henle; '4', distal convoluted tubule; '5', collecting duct. The orange region indicates the possible origins of SS-USCs, and the cyan region indicates the possible origins of RS-USCs.

analyzed (Figure 4). They had similar expression patterns for CD24, CD29, CD34, CD44, CD73 and CD90, which is similar with MSCs (Lv et al., 2014), but not for CD133. CD133 is an important stemness biomarker (Yu et al., 2011; Irollo et al., 2013). It has been reported that progenitor cells from adult kidney exhibit expression of CD133 (Sagrinati et al., 2006). According to some publications, USCs were weakly positive for CD133 (Bharadwaj et al., 2011; Pei et al., 2014; Chen et al., 2017), which is consistent with our results for RS-USCs, and the USCs were reported as non-chondrogenic (Pei et al., 2014). USCs have also been found to be negative for CD133 (Guan et al., 2014; Guan et al., 2015), which is consistent with our results for SS-USCs, and the reported USCs were chondrogenic (Guan et al., 2014; Guan et al., 2015). However, in our study, both SS-USCs and RS-USCs showed chondrogenic differentiation ability, possibly due to the culture conditions. Besides, more experiments are needed to demonstrate the availabilities of other cell type differentiation of SS-USCs and RS-USCs, and the application potentials in tissue type-specific reconstruction.

In addition, the origins of USCs remain an interesting question. It has been reported that USCs from a female recipient with a male kidney transplant contained a Y chromosome, thereby confirming that USCs may originate from renal tissues (Bharadwaj et al., 2013). In our study, we analyzed the expression of several renal cell markers in SS-USCs and RS-USCs. As shown in Figure 5A, SS-USCs were positive for VIM, weakly positive for SLC12A1 and UMOD, and negative for KRT18, NPHS1, AQP1, and AQP2, whereas RS-USCs were positive for VIM, partially positive for KRT18, NPHS1, AQP1, SLC12A1, and UMOD, and nearly negative for AQP2. KRT18 is the major constituent of intermediate filament in epithelial cells from tissues including the kidneys (Messai et al., 2010), and it has been reported that cells with differentiation potentials may also be positive for epithelial markers (Wu et al., 2017). Indeed, the RS-USCs expressed epithelial markers and had multi-potent differentiation abilities. The results of immunofluorescence

assay indicated that SS-USCs possibly originate from the renal mesenchyme near the loop of Henle and distal convoluted tubules (Figure 5B), whereas RS-USCs may originate from nephron tubules including the Bowman's capsule to the distal convoluted tubule, but not from the collecting duct (Figure 5B). It is also possible that the SS-USCs and RS-USCs showed these tissue-specific markers due to spontaneous differentiation, indicating different differentiation capability for the two subpopulations under the same culture condition if it is the case. Nevertheless, identification of the origins of various USC subpopulations will provide a better understanding for their biological characteristics. We speculate that SS-USCs are more suitable for bone repair, and that RS-USCs are more suitable for uroepithelium reconstruction.

Primary culture of urine derived cells has also provided a non-invasive way to harvest epithelial cells (Figures S2–S5 in Supporting Information). Indeed, de-differentiated epithelial cells from urine can repair the proximal tubule (Kusaba et al., 2014). Epithelial cells from urine can provide a source for re-programming into iPSCs (Wang et al., 2013; Lee et al., 2014).

In our study, two subpopulations of USCs were identified, and their biological profiles were characterized. However, more research is needed to demonstrate the detailed profiles, such as the immunogenicity and safety of these subpopulations of USCs. Besides, the separation procedures for the subpopulations of urine-derived cells applied in this study were primitive. However, because whether the morphologically distinct cell populations were different is unknown, we separated the cell populations with the easily-practicable single clone digestion assay. In this study, different characteristics of the subpopulations were observed, but unique markers for precise sorting had not been identified yet. In future studies, further characterization of the two USC subpopulations by proteomics analysis will probably provide more detailed insights and contribute to precise sorting.

In conclusion, two morphotypes of USCs have been identified as SS-USC and RS-USC subpopulations. Both subpopulations express stemness-related POU5F1 gene, the SS-USCs have stronger osteogenic and adipogenic differentiation potentials, and the RS-USCs have stronger chondrogenic differentiation potentials. Whilst both types displayed similar clone forming efficiency, the SS-USCs featured a more elongated morphology, a faster proliferation rate, and a greater motility. The SS-USCs and RS-USCs have similar expression patterns for CD24, CD29, CD34, CD44, CD73, CD90 and CD105, although RS-USCs have a higher positive percentage for CD133. The SS-USCs were positive for VIM, weakly positive for SLC12A1 and UMOD, and negative for KRT18, NPHS1, AQP1 and AQP2, thereby indicating a renal mesenchyme origin. The RS-USCs were positive for VIM, partial positive for KRT18, NPHS1, AQP1, SLC12A1 and UMOD, and negative for AQP2, which indicated a nephron tubule origin. These results enhance our understanding of their biological characteristics and provide a basis for further research on USCs-based cytotherapies.

## MATERIALS AND METHODS

### Cell culture

The complete medium for USCs was prepared according to the published protocol with modifications as follows: 50% K-SFM (Gibco, Thermo Fisher Scientific, USA), 33.75% DMEM-HG (Gibco, Thermo Fisher Scientific), 11.25% Ham's F12 (Hyclone, GE Healthcare Bio-Sciences, USA), 5% FBS, supplemented by 5 ng $mL^{-1}$ EGF, 50 ng $mL^{-1}$ BPE, 0.4 μg $mL^{-1}$ hydrocortisone, 5 μg $mL^{-1}$ transferrin, 5 ng $mL^{-1}$ bovine insulin, 0.18 mmol $L^{-1}$ adenine, 2 nmol $L^{-1}$ 3,3,5-Triiodo-L-thyromine, 100 units $mL^{-1}$ penicillin and 100 μg $mL^{-1}$ streptomycin.

Fresh urine samples were collected for primary cultures of urine-derived cells. The samples were centrifuged in 50 mL centrifuge tubes at 400×*g* for 10 min at 25°C. Most of the supernatant was discarded, and 5 mL of liquid was kept in each tube. 40 mL PBS containing 1% penicillin-streptomycin was added into each tube, and the liquid was mixed, which was followed by two further rounds of centrifuging. The supernatant was discarded, and PBS was added. After the final centrifugation, the supernatant was discarded. The precipitated cells (urine derived cells) were resuspended in 5 mL complete medium and seeded in 25 $cm^2$ culture flask. The cells were cultured at 37°C in a humidified incubator with 5% $CO_2$. When cell clones had formed, the culture medium was replaced with fresh medium.

For subculture of urine derived cells with specific morphologies, cell clones were collected by individual digestion (Figure S1 in Supporting Information). Briefly, 10 μL of trypsin was added onto a single clone with distinct morphology. The cells were collected, centrifuged and resuspended, and then re-cultured in a new culture flask. For further subculture, a split ratio of 1:3 was applied. Passage 3 cells were used for the subsequent experiments, if not specified.

### Cell morphology

Cell images were captured with an IX71 microscope imaging system (Olympus, Japan). Cell morphology was measured with ImageJ software.

### RT-qPCR

To determine the transcriptional level of genes, total RNAs

were extracted with RNAiso plus (TaKaRa, Japan) by following the manufacturer's protocol. Reverse transcription was performed with a PrimeScript™ RT reagent Kit with gDNA Eraser (TaKaRa) on a thermocycler (Bio-Rad, USA). qPCR was performed with SYBR® Premix Ex Taq™ II (TaKaRa) by following the manufacturer's protocol on a LightCycler® 96 system (Roche, Switzerland). The primer sequences for each gene were as follows:

GAPDH, forward, 5′-AGACAGCCGCATCTTCTTGT-3′, reverse, 5′-TGATGGCAA-CAATGTCCACT-3′; MYC, forward, 5′-GTCAAGAGGCGAACACACAAC-3′, reverse, 5′-TTGGACGGACAGGATGTATGC-3′; POU5F1, forward, 5′-CAAAGCAGA-AACCCTCGTGC-3′, reverse, 5′-TCTC-ACTCGGTTCTCGATACTG-3′.

The relative gene expression levels were calculated with a $2^{-\Delta\Delta C_t}$ method (Livak and Schmittgen, 2001).

### Multi-differentiation assay

For osteogenic differentiation, USCs were seeded onto glass coverslips in 6-well plates as $6\times10^4$ cells/well and cultured in an osteogenic medium. The osteogenic medium was DMEM-HG plus 10% FBS, 50 μg mL$^{-1}$ ascorbic acid, 0.2 μmol L$^{-1}$ dexamethasone, and 10 mmol L$^{-1}$ of β-glycerophosphate disodium. After 28 d of culture, the cells were fixed with 75% ethanol for 20 min, washed with PBS twice and stained with 0.1% Alizarin red S (Sigma-Aldrich, Merck KGaA, Germany) for 30 min. The images were captured with IX71 microscope imaging system (Olympus).

For adipogenic differentiation, USCs were seeded onto glass coverslips in 6-well plates as $1\times10^5$ cells/well and cultured in an adipogenic medium. The adipogenic medium was DMEM-HG plus 10% FBS, 1 μmol L$^{-1}$ dexamethasone, 10 μg mL$^{-1}$ bovine insulin, 50 μmol L$^{-1}$ indomethacin, and 500 μmol L$^{-1}$ isobutylmethylxanthine. After 28 d of culture, the cells were fixed with 75% ethanol and stained with 0.5% fresh Oil-red O solution (Sigma-Aldrich, Merck KGaA) for 45 min. The images were captured with IX71 microscope imaging system (Olympus).

For chondrogenic differentiation, USCs were seeded onto glass coverslips in 6-well plates as $1.5\times10^5$ cells/well and cultured in a chondrogenic medium (StemPro® Chondrogenesis Differentiation Kit, A1007101, Gibco, Thermo Fisher Scientific, Inc.) according to the manufacturer's protocol. After 24 d of culture, the cells were fixed with 4% formaldehyde, and stained with 1% Alcian Blue solution (G2541, Solarbio, China) for 30 min. The images were captured with IX71 microscope imaging system (Olympus).

### CCK-8 assay

CCK-8 (Dojindo Molecular Technologies, Japan) assay was performed by following the manufacturer's instruction. Briefly, CCK-8 was added into plate wells at 1:10/$V_{cck\text{-}8}$: $V_{medium}$. The plate was incubated at 37°C for 2 h, and the $A_{450}$ was measured immediately with a spectrophotometer (Biotek Instruments, USA).

### Clone forming assay

Cells were seeded into 25 cm$^2$ culture flasks at 800 cells cm$^{-2}$. The culture medium was changed every 3 days. After 15 days of culture, the cell clones were fixed with formalin for 5 min at room temperature and stained with 0.5% crystal violet for 30 min at 37°C. After washing with PBS for 5 times, clones were counted with an IX71 microscope imaging system (Olympus). Clones smaller than 2 mm in diameter were excluded. To calculate the Clone Forming Efficiency (CFE), $N_{clones}$ (the number of clones) and $N_{cells}$ (the number of seeding cells) were applied in the following formula: $CFE=N_{clones}/N_{cells}\times100\%$.

### Wound healing assay

USCs were seeded into 6-well plates at $2\times10^5$ cells/well. When their confluence reached 90%, the cells were scratched with a 1,000 μL pipette tip. The original boundaries of the wounds were marked at the bottom surface of the plate. Cell debris was washed away with PBS. The residual cells were cultured in complete medium containing only 1% FBS for 40 h. The images were captured with an IX71 microscope imaging system (Olympus), and the distances between the wound boundaries before ($D_1$) and after ($D_2$) the healing were measured with Image Pro Plus 6.0. Wound healing rate (WHR) was calculated using the following formula: $WHR=(D_1\text{-}D_2)/D_1\times100\%$. The healing rates of five random microscopic fields were calculated for statistical analysis.

### FCM analysis

Cells were collected by digestion, washed with PBS, resuspended in PBS, and counted. The concentration was adjusted to $2\times10^6$ cells mL$^{-1}$. For FCM analysis of each cell marker, 100 μL cell suspension was incubated with corresponding fluorochrome-conjugated antibody PE Mouse anti-human CD24 (311105, BioLegend, Inc., USA), APC Mouse Anti-Human CD29 (559883, BD Pharmingen™, USA), FITC Mouse Anti-Human CD34 (555821, BD Pharmingen™), FITC Mouse Anti-Human CD44 (555478, BD Pharmingen™), PE Mouse Anti-Human CD73 (550257, BD Pharmingen™), PE-Cy™7 Mouse Anti-Human CD90 (561558, BD Pharmingen™), FITC Mouse anti-Human CD105 (561443, BD Pharmingen™), CD133/1-VioBright FITC, human (130-111-085, Miltenyi Biotec GmbH, Germany) for 30 min at room temperature. Relevant isotype

controls were applied as negative control. The cells were washed with PBS, centrifuged and resuspended in 200 μL PBS. The FCM analysis was performed with Navios Flow Cytometer (Beckman Coulter, Inc., USA).

### Immunocytochemistry

Cells cultured on coverslips were fixed with 4% formaldehyde for 15 min at room temperature and washed with PBS for three times. Permeabilization was performed with 0.5% Triton X-100 for 10 min at room temperature. After washing with PBS for three times, blocking was performed with 1% BSA for 1 h at room temperature. Primary antibodies were as follows: Vimentin (VIM, 1:200 diluted, 14-9897-82, eBioscience, Thermo Fisher Scientific, Inc.); Cytokeratin 18 (KRT18, 1:200 diluted, sc-6259, Santa Cruz Biotechnology, Inc., USA); Nephrin (NPHS1, 1:200 diluted, abs120474, Absin Bioscience Co., Ltd., China); Aquaporin 1 (AQP1, 1:200 diluted, abs123050, Absin Bioscience Co., Ltd); Solute carrier family 12 member 1 (SLC12A1, 1:100 diluted, 18970-1, Proteintech, USA); Uromodulin (UMOD, 1:100 diluted, 11911-1, Proteintech); Aquaporin 2 (AQP2, 1:200 diluted, abs125256, Absin Bioscience Co., Ltd). Primary antibody incubation was performed at 4°C overnight. After washing with PBS for three times, samples were incubated with 1:200 diluted Alexa Fluor® 647 AffiniPure Goat Anti-Mouse IgG (H+L) (115-605-003, Jackson ImmunoResearch Laboratories, Inc., West Grove, PA, USA) or Alexa Fluor® 647 AffiniPure Goat Anti-Rabbit IgG (H+L) (111-605-003, Jackson ImmunoResearch Laboratories, Inc., USA) at 37°C for 1 h. After washing with PBS for three times, the nuclei were stained with DAPI (1 μg $mL^{-1}$) at room temperature for 5 min. After final washing with PBS for five times, the immunofluorescence was photographed with an Axio Imager Z2 microscope (Carl Zeiss Microscopy GmbH, Germany).

### Statistics analysis

Statistics analysis was performed with SPSS 16.0 software. All experiments were repeated at least three times with different cell clones. All results were expressed as mean±SD. Student's *t* test was applied to compare the difference of the groups. $P<0.05$ was considered as significantly different.

**Compliance and ethics** *The author(s) declare that they have no conflict of interest. Human urine samples were collected for experiments with informed consent.*

**Acknowledgements** *The authors thank Dan Long, and Fang-Fang Wang, and Yi Zhang for technical assistance, thank Dr. James G. Ogg for grammatical assistance. This work was supported by the National Key Research & Development Program of China (2017YFC1104702), the National Natural Science Foundation of China (31771065, 31600792, 81473446), the Sichuan Science and Technology Program (2019JDRC0020), and the 1.3.5 project for disciplines of excellence, West China Hospital, Sichuan University (ZYJC18002).*

## References

Alvarez-Gonzalez, C., Duggleby, R., Vagaska, B., Querol, S., Gomez, S.G., Ferretti, P., and Madrigal, A. (2013). Cord blood $Lin^{-}CD45^{-}$ embryonic-like stem cells are a heterogeneous population that lack self-renewal capacity. PLoS ONE 8, e67968.

Bharadwaj, S., Liu, G., Shi, Y., Markert, C., Andersson, K.E., Atala, A., and Zhang, Y. (2011). Characterization of urine-derived stem cells obtained from upper urinary tract for use in cell-based urological tissue engineering. Tissue Eng Part A 17, 2123–2132.

Bharadwaj, S., Liu, G., Shi, Y., Wu, R., Yang, B., He, T., Fan, Y., Lu, X., Zhou, X., Liu, H., et al. (2013). Multipotential differentiation of human urine-derived stem cells: Potential for therapeutic applications in urology. Stem Cells 31, 1840–1856.

Bossolasco, P., Montemurro, T., Cova, L., Zangrossi, S., Calzarossa, C., Buiatiotis, S., Soligo, D., Bosari, S., Silani, V., Deliliers, G.L., et al. (2006). Molecular and phenotypic characterization of human amniotic fluid cells and their differentiation potential. Cell Res 16, 329–336.

Cao, Z., Wang, D., Li, Y., Xie, W., Wang, X., Tao, L., Wei, Y., Wang, X., and Zhao, L. (2018). Effect of nanoheat stimulation mediated by magnetic nanocomposite hydrogel on the osteogenic differentiation of mesenchymal stem cells. Sci China Life Sci 61, 448–456.

Chen, W., Xie, M., Yang, B., Bharadwaj, S., Song, L., Liu, G., Yi, S., Ye, G., Atala, A., and Zhang, Y. (2017). Skeletal myogenic differentiation of human urine-derived cells as a potential source for skeletal muscle regeneration. J Tissue Eng Regen Med 11, 334–341.

De Coppi, P., Bartsch, G., Siddiqui, M.M., Xu, T., Santos, C.C., Perin, L., Mostoslavsky, G., Serre, A.C., Snyder, E.Y., Yoo, J.J., et al. (2007). Isolation of amniotic stem cell lines with potential for therapy. Nat Biotechnol 25, 100–106.

Gao, P., Jiang, D., Liu, W., Li, H., and Li, Z. (2016). Urine-derived stem cells, a new source of seed cells for tissue engineering. Curr Stem Cell Res Ther 11, 547–553.

Gao, Y., Guo, Y., Duan, A., Cheng, D., Zhang, S., and Wang, H. (2014). Optimization of culture conditions for maintaining porcine induced pluripotent stem cells. DNA Cell Biol 33, 1–11.

Guan, J., Zhang, J., Li, H., Zhu, Z., Guo, S., Niu, X., Wang, Y., and Zhang, C. (2015). Human urine derived stem cells in combination with β-TCP can be applied for bone regeneration. PLoS ONE 10, e0125253.

Guan, J.J., Niu, X., Gong, F.X., Hu, B., Guo, S.C., Lou, Y.L., Zhang, C.Q., Deng, Z.F., and Wang, Y. (2014). Biological characteristics of human-urine-derived stem cells: potential for cell-based therapy in neurology. Tissue Eng Part A 20, 1794–1806.

Han, S., Xiao, Z., Li, X., Zhao, H., Wang, B., Qiu, Z., Li, Z., Mei, X., Xu, B., Fan, C., et al. (2018). Human placenta-derived mesenchymal stem cells loaded on linear ordered collagen scaffold improves functional recovery after completely transected spinal cord injury in canine. Sci China Life Sci 61, 2–13.

Han, Z.C., Du, W.J., Han, Z.B., and Liang, L. (2017). New insights into the heterogeneity and functional diversity of human mesenchymal stem cells. Biomed Mater Eng 28, S29–S45.

Huang, Y.Z., Cai, J.Q., Lv, F.J., Xie, H.L., Yang, Z.M., Huang, Y.C., and Deng, L. (2013). Species variation in the spontaneous calcification of bone marrow-derived mesenchymal stem cells. Cytotherapy 15, 323–329.

Huang, Y.Z., Xie, H.Q., Silini, A., Parolini, O., Zhang, Y., Deng, L., and Huang, Y.C. (2017). Mesenchymal stem/progenitor cells derived from articular cartilage, synovial membrane and synovial fluid for cartilage regeneration: current status and future perspectives. Stem Cell Rev Rep 13, 575–586.

Irollo, E. and Pirozzi, G. (2013). CD133: to be or not to be, is this the real question? Am J Transl Res 5, 563–581.

Ju, X.A., Chen, J., Ding, L., Li, Y.Z., Xiao, F.J., Li, Z.Q., and Guo, Z.K. (2013). A slowly proliferating subpopulation in human umbilical cord mesenchymal stem cells in culture. In Vitro Cell Dev Biol Anim 49, 653–656.

Kitamura, S., Sakurai, H., and Makino, H. (2015). Single adult kidney stem/progenitor cells reconstitute three-dimensional nephron structures *in vitro*. Stem Cells 33, 774–784.

Klimanskaya, I., Chung, Y., Becker, S., Lu, S.J., and Lanza, R. (2006). Human embryonic stem cell lines derived from single blastomeres. Nature 444, 481–485.

Kuroda, Y., Kitada, M., Wakao, S., and Dezawa, M. (2011). Bone marrow mesenchymal cells: how do they contribute to tissue repair and are they really stem cells? Arch Immunol Ther Exp 59, 369–378.

Kusaba, T., Lalli, M., Kramann, R., Kobayashi, A., and Humphreys, B.D. (2014). Differentiated kidney epithelial cells repair injured proximal tubule. Proc Natl Acad Sci USA 111, 1527–1532.

Lee, J.M., Dedhar, S., Kalluri, R., and Thompson, E.W. (2006). The epithelial–mesenchymal transition: new insights in signaling, development, and disease. J Cell Biol 172, 973–981.

Lee, K.I., Kim, H.T., and Hwang, D.Y. (2014). Footprint- and xeno-free human iPSCs derived from urine cells using extracellular matrix-based culture conditions. Biomaterials 35, 8330–8338.

Li, P., Tian, H., Li, Z., Wang, L., Gao, F., Ou, Q., Lian, C., Li, W., Jin, C., Zhang, J., et al. (2016). Subpopulations of bone marrow mesenchymal stem cells exhibit differential effects in delaying retinal degeneration. Curr Mol Med 16, 567–581.

Li, X., Gao, H., Uo, M., Sato, Y., Akasaka, T., Feng, Q., Cui, F., Liu, X., and Watari, F. (2009). Effect of carbon nanotubes on cellular functions *in vitro*. J Biomed Mater Res 91A, 132–139.

Li, X., Huang, Y., Zheng, L., Liu, H., Niu, X., Huang, J., Zhao, F., and Fan, Y. (2014). Effect of substrate stiffness on the functions of rat bone marrow and adipose tissue derived mesenchymal stem cells *in vitro*. J Biomed Mater Res 102, 1092–1101.

Li, X., Liu, H., Niu, X., Fan, Y., Feng, Q., Cui, F., and Watari, F. (2011). Osteogenic differentiation of human adipose-derived stem cells induced by osteoinductive calcium phosphate ceramics. J Biomed Mater Res 97B, 10–19.

Li, X., Liu, H., Niu, X., Yu, B., Fan, Y., Feng, Q., Cui, F., and Watari, F. (2012). The use of carbon nanotubes to induce osteogenic differentiation of human adipose-derived MSCs *in vitro* and ectopic bone formation *in vivo*. Biomaterials 33, 4818–4827.

Livak, K.J., and Schmittgen, T.D. (2001). Analysis of relative gene expression data using real-time quantitative PCR and the $2^{-\Delta\Delta CT}$ method. Methods 25, 402–408.

Lu, Y., Wang, Z., Chen, L., Wang, J., Li, S., Liu, C., and Sun, D. (2018). The *in vitro* differentiation of *GDNF* gene-engineered amniotic fluid-derived stem cells into renal tubular epithelial-like cells. Stem Cells Dev 27, 590–599.

Lv, F.J., Tuan, R.S., Cheung, K.M.C., and Leung, V.Y.L. (2014). Concise review: the surface markers and identity of human mesenchymal stem cells. Stem Cells 32, 1408–1419.

Messai, Y., Noman, M.Z., Derouiche, A., Kourda, N., Akalay, I., Hasmim, M., Stasik, I., Ben Jilani, S., Chebil, M., Caignard, A., et al. (2010). Cytokeratin 18 expression pattern correlates with renal cell carcinoma progression: relationship with Snail. Int J Oncol 36.

Pérez-Silos, V., Camacho-Morales, A., and Fuentes-Mera, L. (2016). Mesenchymal stem cells subpopulations: application for orthopedic regenerative medicine. Stem Cells Int 2016(2), 1–9.

Pei, M., Li, J., Zhang, Y., Liu, G., Wei, L., and Zhang, Y. (2014). Expansion on a matrix deposited by nonchondrogenic urine stem cells strengthens the chondrogenic capacity of repeated-passage bone marrow stromal cells. Cell Tissue Res 356, 391–403.

Phinney, D.G., and Prockop, D.J. (2007). Concise review: mesenchymal stem/multipotent stromal cells: the state of transdifferentiation and modes of tissue repair—current views. Stem Cells 25, 2896–2902.

Puri, M.C., and Nagy, A. (2012). Concise review: embryonic stem cells versus induced pluripotent stem cells: the game is on. Stem Cells 30, 10–14.

Sagrinati, C., Netti, G.S., Mazzinghi, B., Lazzeri, E., Liotta, F., Frosali, F., Ronconi, E., Meini, C., Gacci, M., Squecco, R., et al. (2006). Isolation and characterization of multipotent progenitor cells from the Bowman's capsule of adult human kidneys. J Am Soc Nephrol 17, 2443–2456.

Schäffler, A., and Büchler, C. (2007). Concise review: adipose tissue-derived stromal cells—basic and clinical implications for novel cell-based therapies. Stem Cells 25, 818–827.

Schosserer, M., Reynoso, R., Wally, V., Jug, B., Kantner, V., Weilner, S., Buric, I., Grillari, J., Bauer, J.W., and Grillari-Voglauer, R. (2015). Urine is a novel source of autologous mesenchymal stem cells for patients with epidermolysis bullosa. BMC Res Notes 8, 767.

Tai, M.H., Chang, C.C., Kiupel, M., Webster, J.D., Olson, L.K., and Trosko, J.E. (2005). Oct4 expression in adult human stem cells: evidence in support of the stem cell theory of carcinogenesis. Carcinogenesis 26, 495–502.

Wang, L., Wang, L., Huang, W., Su, H., Xue, Y., Su, Z., Liao, B., Wang, H., Bao, X., Qin, D., et al. (2013). Generation of integration-free neural progenitor cells from cells in human urine. Nat Methods 10, 84–89.

Wu, Q., Fang, T., Lang, H., Chen, M., Shi, P., Pang, X., and Qi, G. (2017). Comparison of the proliferation, migration and angiogenic properties of human amniotic epithelial and mesenchymal stem cells and their effects on endothelial cells. Int J Mol Med 39, 918–926.

Wu, R., Liu, G., Fan, Y., Rohozinski, J., Lu, X., Rodriguez, G., Farney, A., Atala, A., and Zhang, Y. (2013). 249 Human urine-derived stem cells originate from parietal stem cells. J Urol 189.

Yu, X., Lin, Y., Yan, X., Tian, Q., Li, L., and Lin, E.H. (2011). CD133, stem cells, and cancer stem cells: myth or reality? Curr Colorect Cancer Rep 7, 253–259.

Zangrossi, S., Marabese, M., Broggini, M., Giordano, R., D'Erasmo, M., Montelatici, E., Intini, D., Neri, A., Pesce, M., Rebulla, P., et al. (2007). Oct-4 expression in adult human differentiated cells challenges its role as a pure stem cell marker. Stem Cells 25, 1675–1680.

Zhang, D., Wei, G., Li, P., Zhou, X., and Zhang, Y. (2014). Urine-derived stem cells: A novel and versatile progenitor source for cell-based therapy and regenerative medicine. Genes Dis 1, 8–17.

Zhang, Y., McNeill, E., Tian, H., Soker, S., Andersson, K.E., Yoo, J.J., and Atala, A. (2008). Urine derived cells are a potential source for urological tissue reconstruction. J Urol 180, 2226–2233.

## SUPPORTING INFORMATION

**Figure S1** Schematic diagram of primary culture of urine-derived cells and single clone digestion.

**Figure S2** Representative image of urine-derived epithelial cells.

**Figure S3** Urine-derived epithelial cells showed no differentiation potentials.

**Figure S4** Analysis of cell surface markers of urine-derived epithelial cells by flow cytometry.

**Figure S5** Staining for KRT18 in urine-derived epithelial cells.

The supporting information is available online at http://life.scichina.com and https://link.springer.com. The supporting materials are published as submitted, without typesetting or editing. The responsibility for scientific accuracy and content remains entirely with the authors.